RSC Advances

PAPER

View Article Online
View Journal | View Issue

Cite this: *RSC Adv.*, 2020, **10**, 22156

Computational searches for crystal structures of dioxides of group 14 elements (CO_2, SiO_2, GeO_2) under ultrahigh pressure†

Hitoshi Nabata,[a] Makito Takagi,[b] Kenichiro Saita *[c] and Satoshi Maeda *[cdef]

Received 15th April 2020
Accepted 3rd June 2020

DOI: 10.1039/d0ra03359f

rsc.li/rsc-advances

In this study, we focused on the effect of pressure on the crystal structures of dioxides of group 14 elements, *i.e.* SiO_2, GeO_2, and CO_2. Systematic searches for their crystal structures using the artificial force induced reaction method generated 219 and 147, 102 and 63, and 148 and 76 structures for SiO_2, GeO_2, and CO_2, respectively, at 1 and 10^6 atm. At 1 atm, cristobalite-like, quartz, anatase-like, and stishovite were stable structures for SiO_2 and GeO_2. At 10^6 atm, structures of stishovite and $CaCl_2$ type were relatively stable for SiO_2 and GeO_2. At 1 atm of CO_2, molecular crystals were the most stable, whereas, quartz-like and cristobalite-like structures were obtained as stable structures at 10^6 atm. We discuss these pressure dependent structural variations systematically using the obtained structural dataset.

Introduction

The pressure inside the Earth ranges from 1 atm (≈100 kPa) to 3.6 million atm (≈360 GPa).[1] Unusual crystal structures, which cannot be synthesized under ambient pressure, sometimes appear in ultrahigh pressure environments, and it is interesting from chemical and geological viewpoints.

Oxygen and silicon are the two most abundant elements in the Earth's crust, and silicon dioxide (also known as silica) SiO_2 is the most abundant chemical composition in the crust.[2] Therefore, SiO_2 is an important composition in the field of mineralogy. As seen in a SiO_2 phase diagram,[3] SiO_2 has various polymorphs, and their stabilities depend on temperature and pressure. Under normal pressure (1 atm), SiO_2 crystals tend to form a three-dimensional network structure composed of tetrahedral SiO_4 with 4-fold-coordinated Si atoms such as quartz[4,5] and cristobalite.[6,7] In ultrahigh pressure environments (10^5 to 10^6 atm), on the other hand, the crystal structures which contain 6-fold-coordinated Si atoms such as stishovite (rutile-type)[8] and $CaCl_2$-type[9] become dominant. Furthermore, α-PbO_2-type and pyrite-type SiO_2 crystals appear as post-stishovite phases at pressures above 10^6 atm.[10,11]

Germanium dioxide (GeO_2) is a chemical analogue of SiO_2 and several polymorphs have been reported. GeO_2 has similar properties to SiO_2 with respect to temperature and pressure.[12] At 1 atm, GeO_2 can exist in a quartz-like 4-fold-coordinated structure or in a rutile-type 6-fold-coordinated structure.[13] It is reported that GeO_2 can form PbO_2-type[14] and pyrite-type[15] structures under ultrahigh pressure.

It is well known that carbon dioxide (CO_2) crystal exists as a molecular crystal (such as dry ice) under normal pressure. Over the past two decades, however, it has been clarified experimentally that CO_2 can form non-molecular crystal structures like SiO_2 crystals under ultrahigh pressure (>10^5 atm). Phases I (dry ice), II,[16] III,[17] IV,[18,19] and VII[20] have been reported as molecular CO_2 crystal phases, while phases V (tridymite-like[21] and cristobalite-like[22]), VI,[23] and VIII[24] have been reported as non-molecular CO_2 crystal phases.

Previous theoretical studies have successfully reproduced properties of known crystal phases and proposed unidentified crystal structures of AO_2 (A = C, Si, or Ge) under ultrahigh pressure.[25–44] These theoretical predictions were made by stochastic trials including genetic algorithms, or by geometry optimization or MD simulation starting from a known structure or an intuitive initial guess. Since a stable structure in an ultrahigh pressure environment might be completely different from that under normal pressure, especially in the case of CO_2, it is not easy to comprehensively collect all polymorphs of AO_2. Therefore, to this system, an application of a systematic search method which can obtain fully unbiased results without relying on any previous knowledge or human intuition would be beneficial.

[a]*Graduate School of Chemical Sciences and Engineering, Hokkaido University, Sapporo 060-8628, Japan*

[b]*Graduate School of Nanobioscience, Yokohama City University, Yokohama, Kanagawa 236-0027, Japan*

[c]*Department of Chemistry, Faculty of Science, Hokkaido University, Sapporo 060-0810, Japan. E-mail: ksaita@sci.hokudai.ac.jp; smaeda@eis.hokudai.ac.jp*

[d]*Institute for Chemical Reaction Design and Discovery (WPI-ICReDD), Hokkaido University, Sapporo 001-0021, Japan*

[e]*JST, ERATO Maeda Artificial Intelligence for Chemical Reaction Design and Discovery Project, Sapporo 060-0810, Japan*

[f]*Research and Services Division of Materials Data and Integrated System (MaDIS), National Institute for Materials Science (NIMS), Tsukuba 305-0044, Japan*

† Electronic supplementary information (ESI) available: All obtained structures of the A_6O_{12} unit cell in the Cartesian representation. See DOI: 10.1039/d0ra03359f

We have developed a single component artificial force induced reaction (SC-AFIR) method as an automated reaction path search method for molecular systems.[45] The SC-AFIR method computes approximate reaction paths called AFIR paths starting from a stable structure to the other stable structures systematically without needing any arbitrary input like collective variables. By applying the SC-AFIR method to newly found stable structures one after another, a so-called reaction path network on which all stable structures are linked through there interconversion pathways can be generated automatically. The SC-AFIR method is available not only in molecular systems but also in crystalline systems by adopting the periodic boundary conditions (PBC/SC-AFIR),[46] where the PBC/SC-AFIR method computes AFIR paths for phase transitions between stable crystalline phases.

In this study, by using the PBC/SC-AFIR method, we theoretically explored AO_2 (A = C, Si, or Ge) crystal structures at 1 and 10^6 atm respectively. The stable structures (crystal phases) at each pressure and their properties, as the enthalpies and volumes, were discussed. Furthermore, changes of the stability of each crystal structure depending on pressure were discussed, by performing re-optimization of the obtained structures by the systematic searches at 1, 1×10^5, 3×10^5, 6×10^5, and 1×10^6 atm. Using the resultant structural data, similarities and differences among the dioxides of group 14 elements were discussed. Moreover, through these applications, the performance of the PBC/SC-AFIR method was demonstrated.

Methods

The density functional theory (DFT) calculation with the Perdew–Burke–Ernzerhof (PBE) functional and the DZP basis set implemented in SIESTA 4.0 program[47] was used for calculating the potential energy and its gradient. The pseudopotentials were prepared using the parameters in the GGA pseudopotential database;[48] the non-relativistic pseudopotential which includes the nonlinear core correction (NLCC) was applied to a silicon atom, but the nonrelativistic pseudopotential without NLCC was applied to a carbon or an oxygen atom. For germanium atom, the relativistic pseudopotential with NLCC was used. The Fermi–Dirac function was used for the electron smearing (the Gaussian smearing), and the electronic temperature was set to 300 K. The spin state was not fixed. The Monkhorst–Pack grid, which decides k-point sampling, and the mesh cutoff were set to $2 \times 2 \times 2$ and 100 Ry., respectively.

The systematic explorations of the crystal structures were performed by using the PBC/SC-AFIR method[46] implemented in the GRRM program.[49] In the method, the artificial force, which was defined by the AFIR function, was added between two systematically chosen fragments in the given system, and then structural deformations were induced systematically. The AFIR method is available not only in isolated molecular systems but also periodic systems. Here, the SC-AFIR algorithm was used, and the model collision energy parameter γ was set to 1000.0 kJ mol^{-1}. The all atoms in the unit cell were chosen as the target in the SC-AFIR algorithm. No symmetrical restrictions were considered. In this study, compositions A_2O_4 and A_3O_6 (A = C, Si, or Ge) in a unit cell were taken into account. Eight initial structures were randomly generated for each composition. A search was terminated if the last $3n$ AFIR paths did not update the set of the lowest n equilibrium (EQ) structures (n is the number of atoms in the unit cell). All obtained EQs in the A_2O_4 and A_3O_6 unit cells were extended to generate structures in the A_6O_{12} unit cell and reoptimized in the A_6O_{12} unit cell to obtain the final dataset in the A_6O_{12} unit cell. Therefore, all structures presented below are optimized structures in the A_6O_{12} unit cell. To consider pressure effect, the structure searches and further geometry optimizations were performed on the function of the enthalpy $E + PV$ rather than the electronic (potential) energy E, where P is the pressure and V is the volume.[50] In this study, 1 or 10^6 atm was applied as the constant values of P in the structure searches. All obtained structures are available in the ESI.†

Results and discussion

At 1 atm, 219, 102, and 148 equilibrium (EQ) structures were obtained by our systematic searches for CO_2, SiO_2, and GeO_2, respectively. Fig. 1 shows relatively stable structures among the obtained EQ structures at 1 atm. The EQ structures were labeled in ascending order (from zero) of the enthalpy, and the value of enthalpy is the relative to the lowest enthalpy structure in each composition. The lowest enthalpy structure of CO_2 (**EQ-CO_2 0**, Fig. 1(a)), which was obtained under 1 atm, was a molecular crystal known as phase III. Many patterns with different orientations and densities were obtained, and they were lying at the low enthalpy region (~0.23 eV/CO_2). Molecular crystal structures containing 1,3-dioxetanedione and 1,2-dioxetanedione were also found (**EQ-CO_2 174**, Fig. 1(b)). Linear CO_2 chain crystal structures were appeared as the non-molecular crystals of CO_2, even under 1 atm (**EQ-CO_2 182**, Fig. 1(c)). In the case of SiO_2, the lowest enthalpy structure was a cristobalite-like structure, which had a tetrahedral SiO_4 network (**EQ-SiO_2 0**, Fig. 1(d)). The second lowest enthalpy structure was rutile-type structure, stishovite (**EQ-SiO_2 1**, Fig. 1(e)). Stishovite has an octahedral SiO_6 network. The structure of quartz was obtained as the third most stable structure (**EQ-SiO_2 6**, Fig. 1(f)). Note that the structures, such as α-cristobalite, tridymite, and coesite, could not be described by the small unit cells adopted during the searches. In the case of GeO_2, the lowest enthalpy structure was a six-coordinated $CaCl_2$-type structure (**EQ-GeO_2 0**, Fig. 1(g)), and the second lowest enthalpy structure was rutile-type structure (**EQ-GeO_2 1**, Fig. 1(h)). At 1 atm, their enthalpies were almost same. The anatase-type structure (**EQ-GeO_2 3**, Fig. 1(i)) was obtained as the third lowest enthalpy structure. Four-coordinated crystal structures such as quartz-like and cristobalite-like structures were also found, however, the stability of these structures was different from in the case of SiO_2. At 1 atm, the relative enthalpy of 4-fold-coordinated GeO_2 crystal structures was higher than 6-fold structures.

Under 10^6 atm, 147, 63, and 76 EQ structures were obtained for CO_2, SiO_2, and GeO_2 respectively. Relatively stable structures among the obtained EQ structures at 10^6 atm are shown in Fig. 2. The EQs obtained at 10^6 atm are labeled with a prime symbol. The enthalpy values are relative to the most stable EQ of

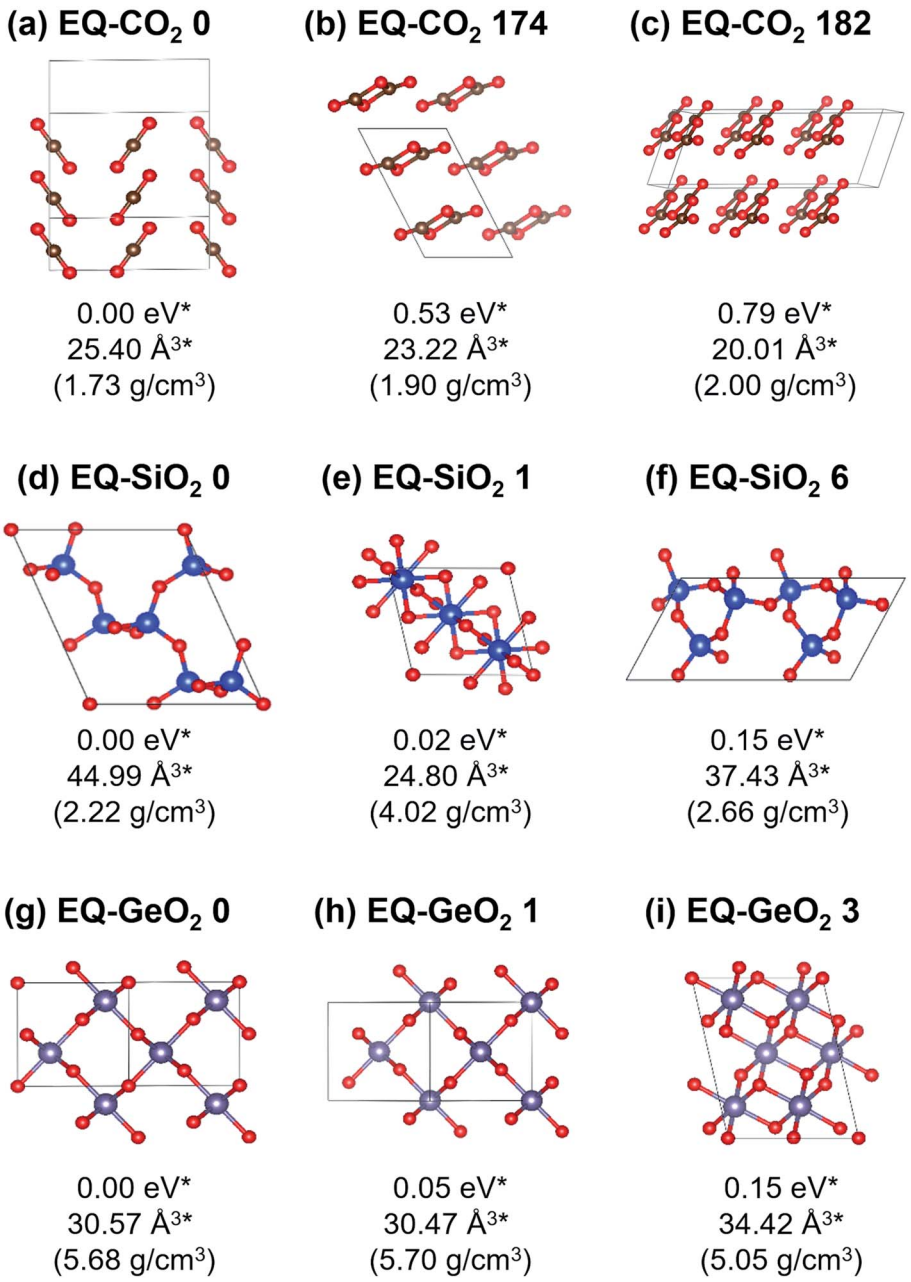

Fig. 1 Relatively stable structures among the obtained crystal structures at 1 atm. (a) CO_2 molecular, (b) non-CO_2 molecular, (c) planar CO_2 chain, (d) 4-fold cristobalite-like, (e) 6-fold stishovite-like, (f) 4-fold quartz, (g) 6-fold $CaCl_2$-type, (h) 6-fold rutile-type, (i) 6-fold anatase-type, *Per AO_2 (A = C, Si, or Ge) unit.

each composition at 10^6 atm. All structures obtained at 10^6 atm had smaller volumes per unit composition, higher densities, and higher enthalpies than those obtained at 1 atm, because 10^6 atm of pressure corresponds to 0.6325 eV $Å^{-3}$. This means if **EQ-CO_2 0** (25.40 $Å^3/CO_2$), which is stable at 1 atm, was put under 10^6 atm, then the *PV* term of the enthalpy increased by 16.07 eV/CO_2. The larger volume unit cell, the *PV* term of the enthalpy becomes much larger. For CO_2, the lowest enthalpy EQ structure under 10^6 atm was a 4-fold-coordinated cristobalite-like structure (**EQ′-CO_2 0**, Fig. 2(a)). This structure was similar to the most stable EQ structure in SiO_2 at 1 atm, but its density is higher than the case of SiO_2. The second lowest enthalpy structure was a layered CO_2 structure with 4-coordinated CO_4 (**EQ′-CO_2 5**, Fig. 2(b)). Such layered structures were also observed in SiO_2 and GeO_2 at 1 atm. The quartz-like structure was also obtained as the third lowest enthalpy structure (**EQ′-CO_2 7**, Fig. 2(c)). The lowest enthalpy structure of SiO_2 under 10^6 atm was a 6-fold-coordinated $CaCl_2$-type structure (**EQ′-SiO_2 0**, Fig. 2(d)). The α-PbO_2-like structure (**EQ′-SiO_2 4**, Fig. 2(e)) was also stable. The anatase-type structure was obtained, but it had relatively high enthalpy (**EQ′-SiO_2 18**, Fig. 2(f)). In contrast to the case of 1 atm, the stishovite structure was not found in 6-fold-

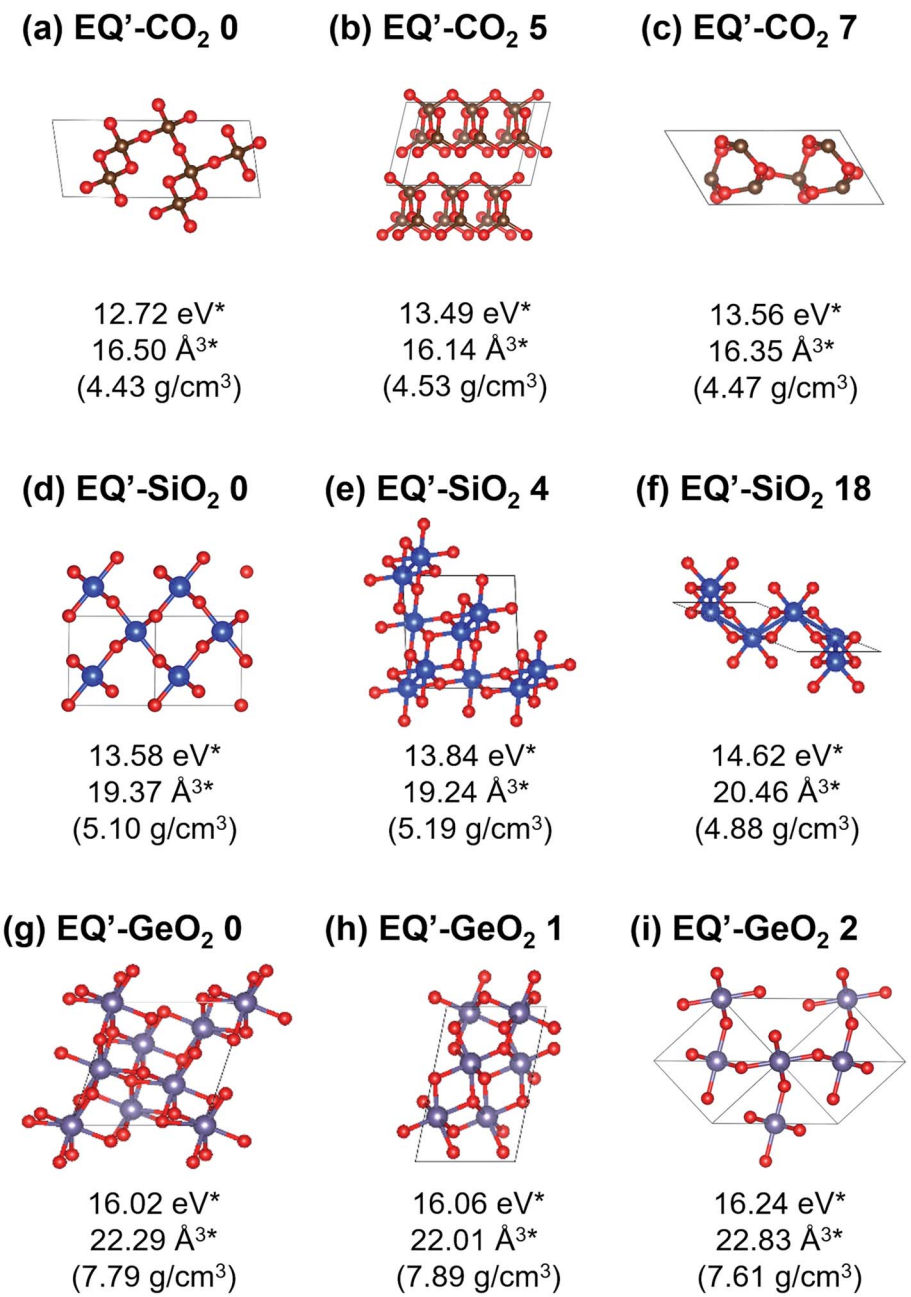

Fig. 2 Relatively stable structures among the obtained crystal structures at 10^6 atm. (a) 4-fold coordinated 3D-network (cristobalite-like), (b) layered CO_2, (c) 4-fold coordinated 3D-network (quartz-like), (d) 6-fold $CaCl_2$-type, (e) 6-fold α-PbO_2-like, (f) 6-fold anatase-type, (g) 7-fold coordinated, (h) 6-fold pyrite-like, (i) 6-fold $CaCl_2$-type. *Per AO_2 (A = C, Si, or Ge) unit.

coordinated structures, and any 4-fold-coordinated structures as well. The lowest enthalpy EQ structure in GeO_2 under 10^6 atm was a 7-fold-coordinated structure which has distorted augmented triangular prism structure (**EQ′-GeO_2 0**, Fig. 2(g)). The 6-fold pyrite-like (**EQ′-GeO_2 1**, Fig. 2(h)) and $CaCl_2$-type (**EQ′-GeO_2 2**, Fig. 2(i)) structures were appeared as the second and the third lowest enthalpy structures at 10^6 atm. The α-PbO_2-like structure (16.43 eV/GeO_2) was also stable (**EQ′-GeO_2 4**).

For the group 14 dioxide systems, many crystalline phases have been reported both experimentally and theoretically.[4–32] Previous theoretical studies have been done by various ways including applications of sophisticated stochastic methods such as USPEX (Universal Structure Predictor: Evolutionary Xtallography),[42] CALYPSO (Crystal structure AnaLYsis by Particle Swarm Optimization),[43] and SSW (Stochastic Surface Walking).[41] To the best of our knowledge, our systematic structure searches generated all known crystal structure types at ~1 or ~10^6 atm that can be expressed within the A_2O_4 and A_3O_6 unit cells (A = C, Si, or Ge). Structures missed by our searches can be categorized into two types: (A) structures that cannot be expressed within the A_2O_4 and A_3O_6 unit cells and (B) structures that are stable only under higher pressure than 10^6 atm. As

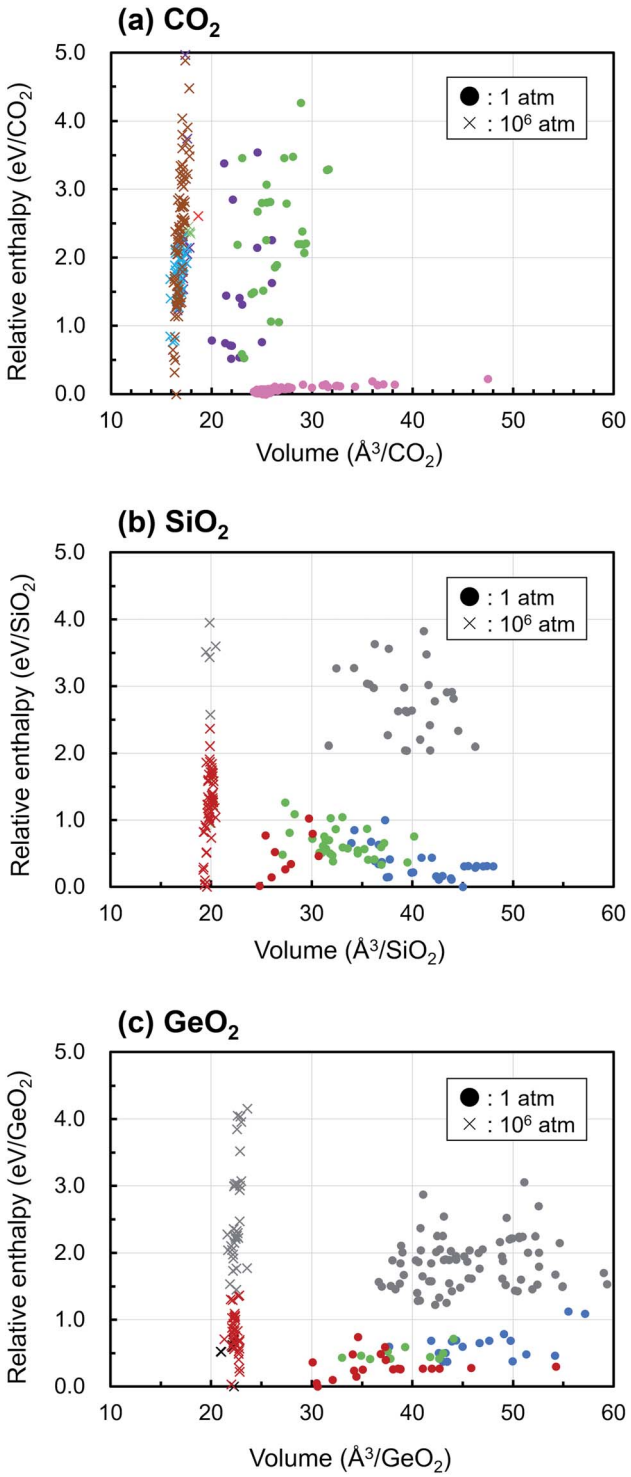

Fig. 3 Scatter plot of relative enthalpies against volumes for obtained AO_2 (A = C, Si, or Ge) structures at 1 atm (circles, ●) and 10^6 atm (cross marks, ×). In figure (a), colors represent CO_2 molecular (pink), non-CO_2 molecular (light green), linear CO_2 chain (purple), 2D-layered (light blue), and 4-fold-coordinated 3D-network (blown) structures, respectively. In figure (b) and (c), colors represent types of structures: 4-fold-coordinated (blue), 5-fold-coordinated (green), 6-fold-coordinated (red), 7-fold-coordinated (black), and O–O bonded (gray) structures, respectively. The relative enthalpy of the most stable structure at 10^6 atm is higher by 12.72 eV/CO_2, 13.58 eV/SiO_2, 16.02 eV/GeO_2 than at 1 atm, respectively.

already noted above, some stable SiO_2 crystals such as α-cristobalite, tridymite, and coesite fall into the category (A). The exact α-PbO_2-type[10] and pyrite-type[11] structures also fall into the category (A). The post-pyrite phases such as cotunnite-type and Fe_2P-type reported for SiO_2 (ref. 35 and 39) and 6-fold-coordinated crystal structures of CO_2 (ref. 30) discovered at higher pressure conditions fall into the category (B). This does not mean the PBC/SC-AFIR method cannot find these structures with any computational setting. These were missed just because of the computational settings, *i.e.* the unit cell sizes and the pressure, adopted in this study. It should also be noted that our searches yielded a number of unreported metastable structures for each composition. Among structures described above, the crystal structures of CO_2 containing 1,3-dioxetanedione and 1,2-dioxetanedione found at 1 atm and 4-fold-coordinated and 6-fold-coordinated layered structures of the three compositions are those newly found by our searches. Also, the 7-fold-coordinated structure of GeO_2 taking distorted augmented triangular prism frame found at 10^6 atm is a newly found relatively stable structure. These results demonstrated usefulness of the PBC/SC-AFIR method in exploration of unknown crystal structures under an arbitrary pressure.

Fig. 3 displays the enthalpy-volume distributions of the obtained EQ structures, where the EQ structures obtained under 1 and 10^6 atm were plotted with circles and with cross marks, respectively. The values of enthalpy are relative to that of the lowest EQ structure at each pressure. In Figure 3(a), 173 of 219 EQ structures were classified as the CO_2 molecular crystal taking different molecular arrangements, which was represented by "dry ice" and they were lying at the low enthalpy region (~0.23 eV/CO_2). In the region of smaller volume and higher enthalpy, other dioxetanedione molecule crystal and linear CO_2 chain crystal structures distribute at 1 atm. Under 10^6 atm, only one EQ structure, which was located at 2.61 eV/CO_2, corresponded to the molecular crystal, and it contained linear CO_2 molecules. Most of EQ structures have dense 3D network structure at 10^6 atm, and molecular crystals become thermodynamically unfavorable. SiO_2 crystals acquire 4-fold-coordinated three-dimensional network structures and 6-fold-coordinated rutile-type structures under 1 atm, and they show wide distribution of volume. Under 1 atm, various densities of SiO_2 crystal structures exist in thermodynamically stable region. On the other hand, at 10^6 atm, only post-stishovite phases, 6-fold-coordinated $CaCl_2$-type, and α-PbO_2-like structures are relatively stable. These structures are obtained in GeO_2 at 1 atm. Although GeO_2 shows similar behavior to SiO_2, the relative enthalpy of 4-fold-coordinated structure is higher than that of 6-fold-coordinated structure at 1 atm. Under 10^6 atm, 7-fold-coordinated structures appear and high dense 6-fold-coordinated structures such as pyrite-like, $CaCl_2$-type, and α-PbO_2-like are relatively stable.

For all compositions, the ultrahigh pressure makes the volume of crystal structure to small, and this causes reducing the number of EQ structures and the volume variation of structures. As a result, the density of crystal increases and the more highly coordinated structures become stable. For example, in the case of CO_2, the EQ structures which were

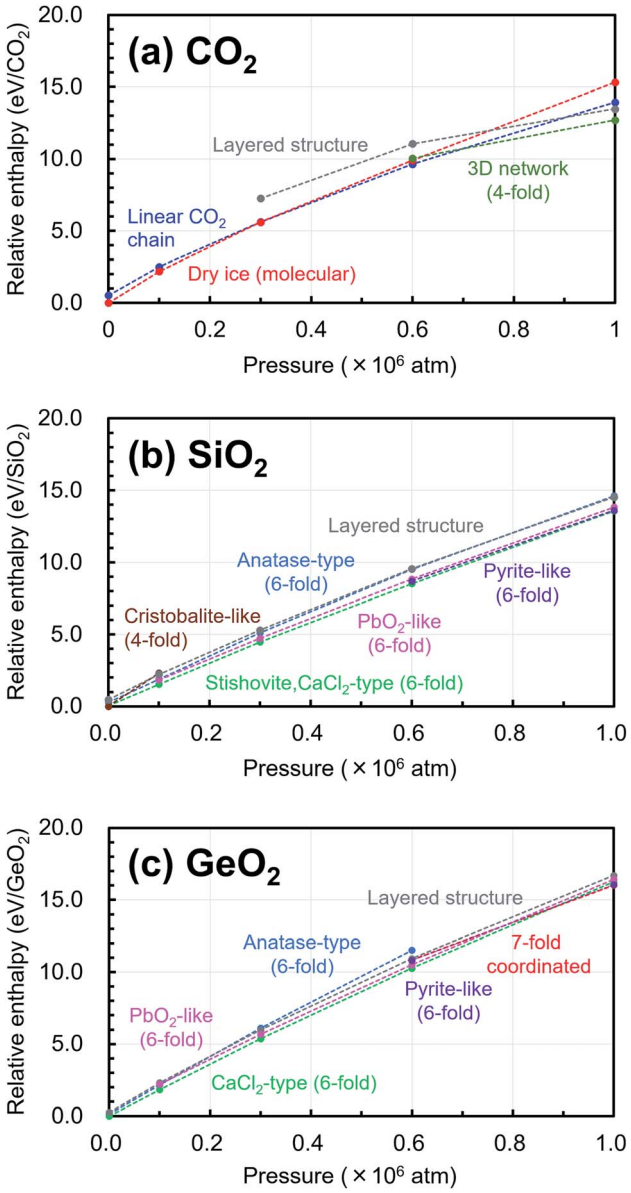

Fig. 4 Trends in the relative stability of structure for pressure in the range of 1 atm to 10^6 atm relative to the most stable structure under 1 atm are shown in (a) CO_2, (b) SiO_2, (c) GeO_2.

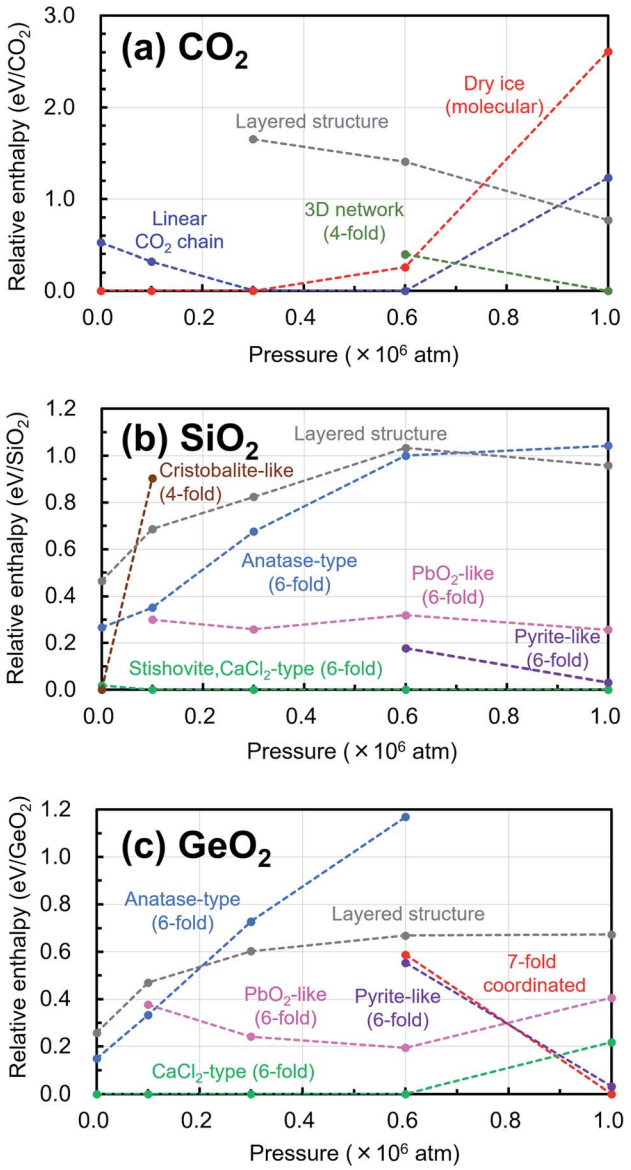

Fig. 5 Trends in the relative enthalpy values relative to the most stable structure under each pressure are shown in (a) CO_2, (b) SiO_2, (c) GeO_2.

obtained at 10^6 atm were located between 12.7–18 eV/CO_2 region relative to at 1 atm, because 10^6 atm of pressure corresponds to 0.6325 eV Å^{-3}, as described above. The relative enthalpy of the most stable structure at 10^6 atm is higher by 12.72 eV/CO_2, 13.58 eV/SiO_2, 16.02 eV/GeO_2 than at 1 atm, respectively. So that the lower density structure such as molecular crystal almost disappeared at 10^6 atm.

In addition, the changes of the relative enthalpy from 1 atm to 10^6 atm were investigated by further structural optimization calculations with different pressures for the EQ structures obtained by the searches. The re-optimizations of the EQ structures obtained under 1 atm were performed by gradually increasing the pressure to 1×10^5, 3×10^5, 6×10^5, and, 1×10^6 atm, while the re-optimizations of the EQ structures obtained under 10^6 atm were carried out by decreasing the pressure *vice versa*. The newly obtained lists of EQ structures at each pressure were merged. The trends in the relative stability of structure for pressure in the range of 1 to 10^6 atm are shown in Fig. 4. For better understanding of these trends, the changes of the relative enthalpy relative to the most stable EQ at each pressure are also shown in Fig. 5. In the case of CO_2, the dry ice crystal has the most stable structure at 1 atm, but at 3×10^5 atm, the relative enthalpy is similar to that of linear CO_2 chain crystal, and at 6×10^5 atm, the linear CO_2 chain crystal has the most stable structure. At 1×10^6 atm, both molecular and linear CO_2 crystals become unstable, and the structure with 3D network structures become relatively stable. Such plots of relative enthalpy change show the transition of stable crystal phases. For SiO_2, at 1 atm, 4-fold-coordinated crystal structures

such as cristobalite-like are relatively stable, and the stishovite is also stable. It changes to the denser $CaCl_2$ structure as the pressure increases, and the $CaCl_2$-type structure was stable even at 10^6 atm. In the 6-fold-coordinated crystal phases, the anatase-type crystal, which has a sparse three-dimensional structure, becomes relatively unstable with increasing pressure, and the dense pyrite-like structure becomes relatively stable. The behavior of 6-fold-coordinated GeO_2 crystals is similar to that of SiO_2. At low pressure, the $CaCl_2$-type structure is relatively stable, as is the case with SiO_2, but at high pressure, the pyrite-type structure and the 7-fold-coordinated structure are relatively stable.

Under ultrahigh pressure, CO_2 has crystal phases similar to SiO_2 under atmospheric pressure. Also, SiO_2 in ultrahigh pressure has crystal phases similar to GeO_2 under atmospheric pressure. This means that crystals of dioxide of a group 14 element exhibit similar properties to those of the next heavier element among the same group by applying ultrahigh pressure. Because a heavier element has a larger atomic radius than a lighter element, it can form structures of higher coordination. Under high pressure, more stable (lower enthalpy) structures should have smaller volume, and the effect of the atomic radius is strongly reflected in the trends of relative stability of crystal structures.

Finally, we summarize limitations of the present study. One is the A_2O_4 and A_3O_6 unit cells adopted in the automated searches. Due to the small unit cells, some known crystal phases that need a larger unit cell are excluded from the obtained crystal structure data. Second is the lack of the thermal effects on the stability. Third is computational errors arisen from computational parameters such as DFT functional and orbital basis functions adopted in this study. Due to the second and third limitations, the stability order among crystal structures discussed above may differ from those by the more accurate calculations taking account of the thermal effects. However, for all the in total >1000 crystal structures obtained over five different pressure conditions, it will take huge computational costs to perform accurate calculations taking account of the thermal effects. Although such calculations may be done for a few specific structures, it is beyond the scope of this paper which aimed to survey the overall trends in structural changes depending on pressure in different group 14 dioxide crystals.

Conclusions

In this study, unbiased searches for crystal structures of dioxides of group 14 elements, SiO_2, GeO_2, and CO_2 were performed using the PBC/SC-AFIR method. A number of crystal structures including known structures have been obtained by our systematic searches. Moreover, some unreported structural phases were predicted as output of the present searches. These results encourage further applications of the PBC/SC-AFIR method to similar targets.

Using the obtained structural data list, we focused on the effect of pressure on the crystal structures. The results of crystal structural searches under the ambient pressure and ultrahigh pressure were successfully compared by considering the enthalpy. Comparisons were also made among the three dioxides, and structural similarity in crystal structures at different pressures was discussed. These results suggest that crystals of dioxide of a group 14 element shows similar properties to those of the next heavier element among the same group by applying ultrahigh pressure. This means that under ultrahigh pressure, CO_2 has crystal phases similar to SiO_2 under atmospheric pressure, and under ultrahigh pressure, SiO_2 has crystal phases similar to GeO_2 under atmospheric pressure.

Conflicts of interest

The authors declare no competing financial interests.

Acknowledgements

Most parts of the computations were performed using Research Center for Computational Science (RCCS), Okazaki, Japan. MT was supported by JSPS Research Fellowships for Young Scientists (PD). This work was supported by JST-CREST (No. JPMJCR14L5), JST-ERATO (No. JPMJER1903), and JSPS-WPI.

Notes and references

1 A. M. Dziewonski and D. L. Anderson, *Phys. Earth Planet. Inter.*, 1981, **25**, 297–356, DOI: 10.1016/0031-9201(81)90046-7.
2 S. R. Taylor and S. M. McLennan, *Philos. Trans. R. Soc., A*, 1981, **301**, 381–399, DOI: 10.1098/rsta.1981.0119.
3 M. Kayama, H. Nagaoka and T. Niihara, *Minerals*, 2018, **8**, 267, DOI: 10.3390/min8070267.
4 K. J. Kingma, H.-K. Mao and R. J. Hemley, *High Pres. Res.*, 1996, **14**, 363–374, DOI: 10.1080/08957959608201422.
5 R. J. Hemley, A. P. Jephcoat, H. K. Mao, L. C. Ming and M. H. Manghnani, *Nature*, 1988, **334**, 52–54, DOI: 10.1038/334052a0.
6 Y. Tsuchida and T. Yagi, *Nature*, 1990, **347**, 267–269, DOI: 10.1038/347267a0.
7 D. M. Hatch and S. Ghose, *Phys. Chem. Miner.*, 1991, **17**, 554–562, DOI: 10.1007/BF00202234.
8 E. C. T. Chao, J. J. Fahey, J. Littler and D. J. Milton, *J. Geophys. Res.*, 1962, **67**, 419–421, DOI: 10.1029/JZ067i001p00419.
9 K. J. Kingma, R. E. Cohen, R. J. Hemley and H.-K. Mao, *Nature*, 1995, **374**, 243–245, DOI: 10.1038/374243a0.
10 L. S. Dubrovinsky, N. A. Dubrovinskaia, V. Prakapenka, F. Seifert, F. Langenhorst, V. Dmitriev, H.-P. Weber and T. Le Bihan, *Phys. Earth Planet. Inter.*, 2004, **143–144**, 231–240, DOI: 10.1016/j.pepi.2003.06.006.
11 Y. Kuwayama, K. Hirose, N. Sata and Y. Ohishi, *Phys. Chem. Miner.*, 2011, **38**, 591–597, DOI: 10.1007/s00269-011-0431-6.
12 J. P. Itie, A. Polian, G. Calas, J. Petiau, A. Fontaine and H. Tolentino, *Phys. Rev. Lett.*, 1989, **63**, 398–401, DOI: 10.1103/PhysRevLett.63.398.
13 A. W. Laubengayer and D. S. Morton, *J. Am. Chem. Soc.*, 1932, **54**, 2303–2320, DOI: 10.1021/ja01345a019.
14 V. B. Prakapenka, L. S. Dubrovinsky, G. Shen, M. L. Rivers, S. R. Sutton, V. Dmitriev, H.-P. Weber and T. Le Bihan,

Phys. Rev. B: Condens. Matter Mater. Phys., 2003, **67**, 132101/1–132101/4, DOI: 10.1103/PhysRevB.67.132101.

15 S. Ono, T. Tsuchiya, K. Hirose and Y. Ohishi, *Phys. Rev. B: Condens. Matter Mater. Phys.*, 2003, **68**, 134108/1–134108/7, DOI: 10.1103/PhysRevB.68.134108.

16 C. S. Yoo, H. Kohlmann, H. Cynn, M. F. Nicol, V. Iota and T. Le Bihan, *Phys. Rev. B: Condens. Matter Mater. Phys.*, 2002, **65**, 104103/1–104103/6, DOI: 10.1103/PhysRevB.65.104103.

17 R. C. Hanson, *J. Phys. Chem.*, 1985, **89**, 4499–4501, DOI: 10.1021/j100267a019.

18 J.-H. Park, C. S. Yoo, V. Iota, H. Cynn, M. F. Nicol and T. Le Bihan, *Phys. Rev. B: Condens. Matter Mater. Phys.*, 2003, **68**, 014107/1–014107/9, DOI: 10.1103/PhysRevB.68.014107.

19 F. Datchi, V. M. Giordano, P. Munsch and A. M. Saitta, *Phys. Rev. Lett.*, 2009, **103**, 185701/1–185701/4, DOI: 10.1103/PhysRevLett.103.185701.

20 W. Sontising, Y. N. Heit, J. L. McKinley and G. J. O. Beran, *Chem. Sci.*, 2017, **8**, 7374–7382, DOI: 10.1039/C7SC03267F.

21 C. S. Yoo, H. Cynn, F. Gygi, G. Galli, V. Iota, M. Nicol, S. Carlson, D. Häusermann and C. Mailhiot, *Phys. Rev. Lett.*, 1999, **83**, 5527–5530, DOI: 10.1103/PhysRevLett.83.5527.

22 M. Santoro, F. A. Gorelli, R. Bini, J. Haines, O. Cambon, C. Levelut, J. A. Montoya and S. Scandolo, *Proc. Natl. Acad. Sci. U. S. A.*, 2012, **109**, 5176–5179, DOI: 10.1073/pnas.1118791109.

23 V. Iota, C. S. Yoo, J. H. Klepeis, Z. Jenei, W. Evans and H. Cynn, *Nat. Mater.*, 2007, **6**, 34–38, DOI: 10.1038/nmat1800.

24 A. Sengupta and C.-S. Yoo, *Phys. Rev. B: Condens. Matter Mater. Phys.*, 2009, **80**, 014118/1–014118/6, DOI: 10.1103/PhysRevB.80.014118.

25 B. Holm, R. Ahuja, A. Belonoshko and B. Johansson, *Phys. Rev. Lett.*, 2000, **85**, 1258–1261, DOI: 10.1103/PhysRevLett.85.1258.

26 I. Gimondi and M. Salvalaglio, *J. Chem. Phys.*, 2017, **147**, 114502/1–114502/11, DOI: 10.1063/1.4993701.

27 Y. Han, J. Liu, L. Huang, X. He and J. Li, *npj Quantum Mater.*, 2019, **4**, 10/1–10/7, DOI: 10.1038/s41535-019-0149-0.

28 J.-H. Parq, S. K. Lee, S.-M. Lee and J. Yu, *J. Phys. Chem. C*, 2016, **120**, 23152–23164, DOI: 10.1021/acs.jpcc.6b07833.

29 J. A. Montoya, R. Rousseau, M. Santoro, F. A. Gorelli and S. Scandolo, *Phys. Rev. Lett.*, 2008, **100**, 163002, DOI: 10.1103/PhysRevLett.100.163002.

30 C. Lu, M. Miao and Y. Ma, *J. Am. Chem. Soc.*, 2013, **135**, 14167–14171, DOI: 10.1021/ja404854x.

31 S. A. Bonev, F. Gygi, T. Ogitsu and G. Galli, *Phys. Rev. Lett.*, 2003, **91**, 065501/1–065501/4, DOI: 10.1103/PhysRevLett.91.065501.

32 X. Yong, H. Liu, M. Wu, Y. Yao, J. S. Tse, R. Dias and C. S. Yoo, *Proc. Natl. Acad. Sci. U. S. A.*, 2016, **113**, 11110–11115, DOI: 10.1073/pnas.1601254113.

33 Q. Y. Hu, J.-F. Shu, A. Cadien, Y. Meng, W. G. Yang, H. W. Sheng and H.-K. Mao, *Nat. Commun.*, 2015, **6**, 6630, DOI: 10.1038/ncomms7630.

34 C. Rajappa, S. B. Sringeri, Y. Subramanian and J. Gopalakrishnan, *J. Chem. Phys.*, 2014, **140**, 244512/1–244512/11, DOI: 10.1063/1.4885141.

35 A. Metsue and T. Tsuchiya, *Phys. Chem. Miner.*, 2012, **39**, 177–187, DOI: 10.1007/s00269-011-0473-9.

36 D. M. Teter, R. J. Hemley, G. Kresse and J. Hafner, *Phys. Rev. Lett.*, 1998, **80**, 2145–2148, DOI: 10.1103/PhysRevLett.80.2145.

37 W. Liu, X. Wu, Y. Liang, C. Liu, C. R. Miranda and S. Scandolo, *Proc. Natl. Acad. Sci. U. S. A.*, 2017, **114**, 12894–12899, DOI: 10.1073/pnas.1710651114.

38 Z. Łodziana, K. Parlinski and J. Hafner, *Phys. Rev. B: Condens. Matter Mater. Phys.*, 2001, **63**, 134106/1–134106/7, DOI: 10.1103/PhysRevB.63.134106.

39 S. Wu, K. Umemoto, M. Ji, C.-Z. Wang, K.-M. Ho and R. M. Wentzcovitch, *Phys. Rev. B: Condens. Matter Mater. Phys.*, 2011, **83**, 184102/1–184102/4, DOI: 10.1103/PhysRevB.83.184102.

40 X.-J. Zhang, C. Shang and Z.-P. Liu, *Phys. Chem. Chem. Phys.*, 2017, **19**, 4725–4733, DOI: 10.1039/c6cp06895b.

41 C. Shang, X.-J. Zhang and Z.-P. Liu, *Phys. Chem. Chem. Phys.*, 2014, **16**, 17845–17856, DOI: 10.1039/C4CP01485E.

42 A. R. Oganov and C. W. Glass, *J. Chem. Phys.*, 2006, **124**, 244704/1–244704/15, DOI: 10.1063/1.2210932.

43 Y. Wang, J. Lv, L. Zhu and Y. Ma, *Phys. Rev. B: Condens. Matter Mater. Phys.*, 2010, **82**, 094116/1–094116/8, DOI: 10.1103/PhysRevB.82.094116.

44 E. Zurek and W. Grochala, *Phys. Chem. Chem. Phys.*, 2015, **17**, 2917–2934, DOI: 10.1039/C4CP04445B.

45 S. Maeda, Y. Harabuchi, M. Takagi, K. Saita, K. Suzuki, T. Ichino, Y. Sumiya, K. Sugiyama and Y. Ono, *J. Comput. Chem.*, 2018, **39**, 233–250, DOI: 10.1002/jcc.25106.

46 M. Takagi, T. Taketsugu, H. Kino, Y. Tateyama, K. Terakura and S. Maeda, *Phys. Rev. B*, 2017, **95**, 184110/1–184110/11, DOI: 10.1103/PhysRevB.95.184110.

47 J. M. Soler, E. Artacho, J. D. Gale, A. García, J. Junquera, P. Ordejón and D. Sánchez-Portal, *J. Phys.: Condens. Matter*, 2002, **14**, 2745–2779, DOI: 10.1088/0953-8984/14/11/302; E. Artacho, J. M. Cela, J. D. Gale, A. García, J. Junquera, R. M. Martin, P. Ordejón, D. Sánchez-Portal, J. M. Soler, *SIESTA 4.0.2*, The Siesta Group, 2018, https://departments.icmab.es/leem/siesta/.

48 *Translation of Abinit's GGA Pseudo Database to Siesta Format*, https://departments.icmab.es/leem/siesta/Databases/Pseudopotentials/periodictable-gga-abinit.html.

49 S. Maeda, K. Ohno and K. Morokuma, *Phys. Chem. Chem. Phys.*, 2013, **15**, 3683–3701, DOI: 10.1039/C3CP44063J; S. Maeda, Y. Harabuchi, Y. Sumiya, M. Takagi, K. Suzuki, K. Sugiyama, Y. Ono, M. Hatanaka, Y. Osada, T. Taketsugu, K. Morokuma and K. Ohno, *GRRM (a developmental version)*, Hokkaido University, 2019.

50 M. Takagi and S. Maeda, *ChemRxiv*, 2020, DOI: 10.26434/chemrxiv.12115581.v.